Modelling the Effects of Realistic Environments in the Nearfield and Farfield of Low Frequency Antennas with 3D FDTD Method

J. Vincent, P. Borderies, V. Gobin, Jean-René Poirier

Modelling the Effects of Realistic Environments in the Nearfield and Farfield of Low Frequency Antennas with 3D FDTD Method

Julien Vincent, Pierre Borderies and Vincent Gobin
Electromagnetic and Radar Department
ONERA
Toulouse, France
julien.vincent@onera.fr

Jean-René Poirier
Université de Toulouse; INPT, CNRS
LAPLACE; ENSEEIHT
Toulouse, France

***Abstract* — Ground wave radiation of Low Frequency Antennas is well known for the canonical case of a flat, azimuthally homogeneous, soil. In this paper, more complex kinds of environment are considered in the surroundings of the antenna or in the far field. Both of them are treated by FDTD. Some realistic environments are studied in the near field zone including forest and slopes. An original methodology is proposed for the far field zone. It rests on the use of the direct numerical integration of Sommerfeld's integrals which is presented also.**

Keywords—FDTD; low frequency antennas; natural environments; Sommerfeld's problem; ground wave

I. INTRODUCTION

Ground wave radiation of Low Frequency Antennas is well known for the canonical case of a flat, azimuthally homogeneous soil. In this paper, more complex kinds of environment are considered in the surroundings of the antenna or in the far field. Both of them are treated by The Finite-Difference in Time Domain (FDTD). Some realistic environments are studied in the near field zone including forest and slopes. An original methodology is proposed for the far field zone. It rests on the use of the direct numerical integration of Sommerfeld integrals which is presented also. FDTD method is a well-known method used for computational electromagnetics [1]. For the aim of this paper, the main advantage of using this technique is the ability to treat materials with any electromagnetic properties and any shape. In a previous paper [2], 2D FDTD is applied to obtain the electric field in the direction of propagation.

In section II, low frequency antennas are placed in a forest and on the top of a hill, the Earth's soil being considered as an infinite homogeneous half-plane elsewhere. In the last part of this paper, the method for computing the effect of discontinuities are computed far from the antennas using numerical integration of Sommerfeld's problem.

II. NEARFIELD MODELING

A. Principles

An inverted L antenna is computed at 100 kHz, geometry of the system is shown on Fig. 1. The antenna is made up off two parts, a radiating wire modelled with Holland formalism [3] and a square shaped metallic ground.

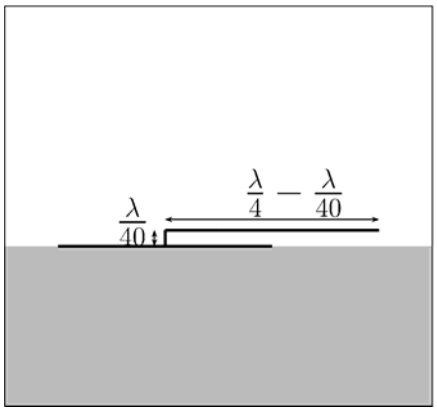

Fig. 1. Geometry of the computed antennas

The Earth's soil is characterized with the dielectric constant ε_{rs} and the conductivity σ_s , which depend of the humidity, see Tab. 1, and can be found in the literature.

TABLE I. DIECLECTRIC CONSTANT AND CONDUCTIVITY FOR DIFFERENCT SOILS

Earth's soils		
	ε_{rs}	σ_s ($S.m^{-1}$)
Dry	5	10^{-4}
Medium wet	15	10^{-3}
Wet	30	10^{-2}

At this frequency range, caution should be taken in extending infinitely the soil so UPML [4] are the boundary conditions applied here.

B. Antenna in a large forest and medium wet soil

With FDTD method, a forest can be represented by a dielectric slab [5] with correspondent dielectric constants ε_{rf} and σ_f. In our case, we chose the medium wet case (ε_{rf} =1.065; σ_f =10^{-3} $S.m^{-1}$) applied for a 25 m high and square shaped (width= 12 km) forest [5]. Fig. 2 shows the results of an

inverted L antennas placed at the center of the forest at the frequency f =100 kHz. The power is sampled at 9 km around the antenna, 1 m over the ground and then normalized by the input power antennas. One can see that the shape of the radiation pattern is not affected by the introduction of the forest but that significant losses occur.

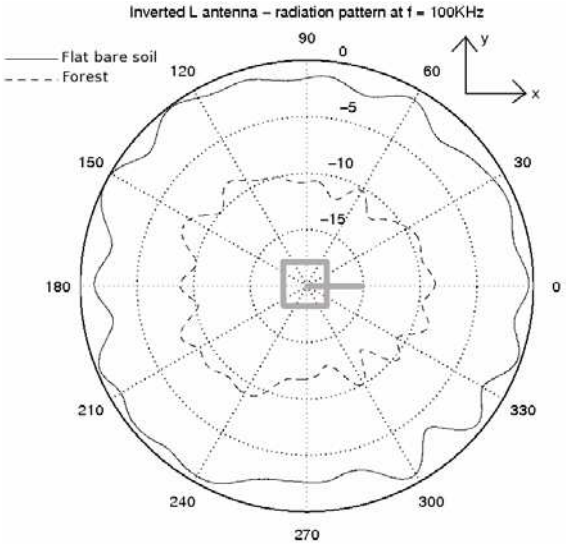

Fig. 2. Simulations of an inverted-L antenna with and without the forest on a medium wet soil.

C. Antenna on the top of a hill and dry soil

An inverted L antenna at the frequency f =100 kHz is placed on the top of a hill made up off 4 square shaped dielectric blocs. All of them are 25 m high, their widths are calculated so as to create an eleven percent average slope and their dielectric constants are the same as the soil. Fig. 3 shows the results of the computation, the power is sampled at 9 km around the antenna, 1 m over the ground and then normalized by the input power antennas. The shape of the radiation pattern is not modified but in this case the radiated power is enhanced.

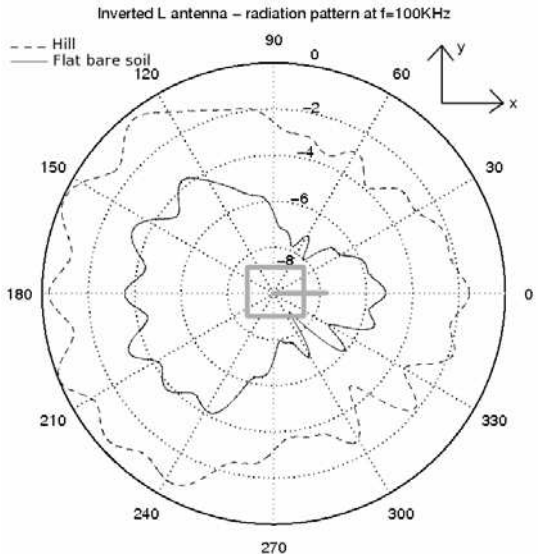

Fig. 3. Simulations of an inverted-L antenna with and without the hill on a dry soil.

III. FAR FIELD MODELING

A. Sommerfeld's problem Principles

In 1909 [6], Sommerfeld calculated the radiation of an infinitesimal vertical electric current element $\mathbf{I} = I_0 dl\mathbf{z}$ situated at a height h above a homogeneous dielectric half-space. The XOY plane separates the two media, the medium 1 is free space in the upper half-space with constants μ_0, ε_0 and soil is the medium 2 in the lower half-space with constants $\mu_1 = \mu_0$, ε_1 and σ_1. The problem is presented on Fig. 4.

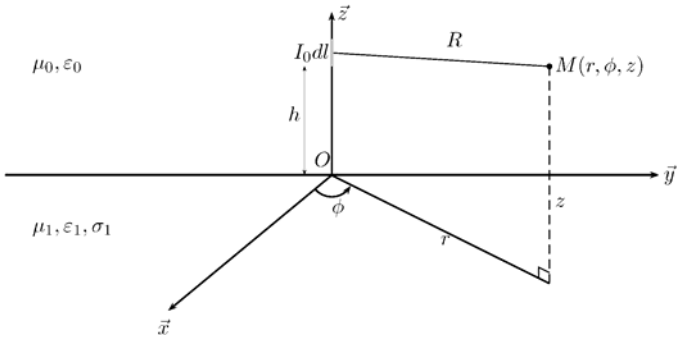

Fig. 4. Vertical z-directed electric current element $I_0 dl$ at height h above planar lossy gruound with electrical parameters $(\mu_1, \varepsilon_1, \sigma_1)$.

Using Maxwell's equation, one can write the relations between Hertz's potential vector $\mathbf{\Pi}$ and the electromagnetic field $\mathbf{E}$ and $\mathbf{H}$. Symmetries and translations show that only the vertical z-component of $\mathbf{\Pi}$ is not equal to zero and depends on the distance r and the height z of the observation point M. This leads to calculate the components $\mathbf{E_\rho}$, $\mathbf{E_z}$ and $\mathbf{H_\varphi}$. The problem is separated into two parts: the source ($\mathbf{\Pi_0}$) and the boundary conditions between medium 1 and medium 2 ($\mathbf{\Pi_1}$ and $\mathbf{\Pi_2}$). The potential vector $\mathbf{\Pi_0}$ created by an electric dipole in air equals to a spherical wave with the magnitude of $(\mu_0 I_0 dl/4\pi)$. It has been shown by Sommerfeld [6] that the spherical wave expanding from a current element $I_0 l$ can be represented by a spectrum of cylindrical waves. Each of which travels as $J_0(\lambda r)$ in the radial r-direction and as $exp[-|z-h|(\lambda^2-k_0^2)^{1/2}]$ in the z-direction with a magnitude of $(\mu_0 I_0 dl/4\pi)\lambda d\lambda/(\lambda^2-k_0^2)^{1/2}$. Here, J_0 refers to the Bessel function of the first kind and k_0 is the free space wavenumber given by $\omega(\mu_0\varepsilon_0)^{1/2}$. Potential Vectors $\mathbf{\Pi_1}$ and $\mathbf{\Pi_2}$ can be written with the same expansion in (1).

$$\text{for } h > z \geq 0:$$

$$\Pi_0(r,z) = \frac{\mu_0 I_0 l}{4\pi}\frac{e^{-jk_0 R}}{R} = \frac{\mu_0 I_0 l}{4\pi}\int_0^{+\infty} J_0(\lambda r)\frac{e^{(z-h)\sqrt{\lambda^2-k_0^2}}}{\sqrt{\lambda^2-k_0^2}}\lambda d\lambda$$

$$\Pi_1(r,z) = \frac{\mu_0 I_0 l}{4\pi}\int_0^{+\infty} J_0(\lambda r)\frac{e^{-(z+h)\sqrt{\lambda^2-k_0^2}}}{\sqrt{\lambda^2-k_0^2}}R_\lambda(\lambda)\lambda d\lambda \qquad (1)$$

$$\text{for } z \leq 0:$$

$$\Pi_2(r,z) = \frac{\mu_0 I_0 l}{4\pi}\int_0^{+\infty} J_0(\lambda r)\frac{e^{z\sqrt{\lambda^2-k_2^2}-h\sqrt{\lambda^2-k_0^2}}}{\sqrt{\lambda^2-k_0^2}}T_\lambda(\lambda)\lambda d\lambda$$

Here, k_2 is the soil wavenumber given by $\omega(\mu_1\varepsilon_1)^{1/2}(1+\sigma_1/j\omega\varepsilon_1)^{1/2}$, $R = (r^2+(z-h)^2)^{1/2}$ is the distance between the dipole and the observation point, R_λ and T_λ are

coefficients which depend on integration variable λ and calculated with the boundary conditions at height $z=0$ in (2). At this height, components $\mathbf{E_\rho}$ and $\mathbf{H_\varphi}$ between the two media have to be continuous.

$$\left.\begin{aligned} \frac{1}{\mu_0}\frac{\partial}{\partial r}(\Pi_0+\Pi_1) &= \frac{1}{\mu_0}\frac{\partial}{\partial r}\Pi_2 \\ \frac{1}{k_0^2}\frac{\partial}{\partial z}\left(\frac{\partial \Pi_0}{\partial r}+\frac{\partial \Pi_1}{\partial r}\right) &= \frac{1}{k_2^2}\frac{\partial}{\partial z}\frac{\partial \Pi_2}{\partial r} \end{aligned}\right\} \quad \text{at } z=0 \text{ and } \forall r \tag{2}$$

This leads to a two equations system (3) with two unknowns R_λ and T_λ.

$$\begin{cases} 1+R_\lambda(\lambda) = T_\lambda(\lambda) \\ \dfrac{\sqrt{\lambda^2-k_0^2}}{k_0^2}\left[1-R_\lambda(\lambda)\right] = \dfrac{\sqrt{\lambda^2-k_2^2}}{k_2^2}T_\lambda(\lambda) \end{cases} \tag{3}$$

The values of R_λ and T_λ are finally obtained in (4). Their expressions can be interpreted as a reflection coefficient R_λ and a transmission coefficient T_λ.

$$\begin{cases} R_\lambda(\lambda) = \dfrac{k_2^2\sqrt{\lambda^2-k_0^2}-k_0^2\sqrt{\lambda^2-k_2^2}}{k_2^2\sqrt{\lambda^2-k_0^2}+k_0^2\sqrt{\lambda^2-k_2^2}} \\ T_\lambda(\lambda) = \dfrac{2k_2^2\sqrt{\lambda^2-k_0^2}}{k_2^2\sqrt{\lambda^2-k_0^2}+k_0^2\sqrt{\lambda^2-k_2^2}} \end{cases} \tag{4}$$

Using these formulas, one obtains in (5) all components of the electromagnetic field **E** and **H** in both media [7].

$$H_\phi^1 = \frac{I_0 l}{4\pi}\left[-\frac{\partial}{\partial r}\frac{e^{-jk_0R}}{R} + \int_0^{+\infty} J_1(\lambda r)\frac{e^{-(z+h)\sqrt{\lambda^2-k_0^2}}}{\sqrt{\lambda^2-k_0^2}}\frac{k_2^2\sqrt{\lambda^2-k_0^2}-k_0^2\sqrt{\lambda^2-k_2^2}}{k_2^2\sqrt{\lambda^2-k_0^2}+k_0^2\sqrt{\lambda^2-k_2^2}}\lambda^2 d\lambda\right]$$

$$E_\rho^1 = -\frac{j\omega\mu_0 I_0 l}{4\pi k_0^2}\left[\frac{\partial^2}{\partial z\partial r}\frac{e^{-jk_0R}}{R} + \int_0^{+\infty} J_1(\lambda r)e^{-(z+h)\sqrt{\lambda^2-k_0^2}}\frac{k_2^2\sqrt{\lambda^2-k_0^2}-k_0^2\sqrt{\lambda^2-k_2^2}}{k_2^2\sqrt{\lambda^2-k_0^2}+k_0^2\sqrt{\lambda^2-k_2^2}}\lambda^2 d\lambda\right]$$

$$E_z^1 = -\frac{j\omega\mu_0 I_0 l}{4\pi k_0^2}\left[\left(\frac{\partial^2}{\partial z^2}+k_0^2\right)\frac{e^{-jk_0R}}{R} + \int_0^{+\infty} J_0(\lambda r)\frac{e^{-(z+h)\sqrt{\lambda^2-k_0^2}}}{\sqrt{\lambda^2-k_0^2}}\frac{k_2^2\sqrt{\lambda^2-k_0^2}-k_0^2\sqrt{\lambda^2-k_2^2}}{k_2^2\sqrt{\lambda^2-k_0^2}+k_0^2\sqrt{\lambda^2-k_2^2}}\lambda^3 d\lambda\right] \tag{5}$$

$$H_\phi^2 = \frac{k_2^2 I_0 l}{2\pi}\int_0^{+\infty} J_1(\lambda r)\frac{e^{z\sqrt{\lambda^2-k_2^2}-h\sqrt{\lambda^2-k_0^2}}}{k_2^2\sqrt{\lambda^2-k_0^2}+k_0^2\sqrt{\lambda^2-k_2^2}}\lambda^2 d\lambda$$

$$E_\rho^2 = \frac{j\omega\mu_0 I_0 l}{2\pi}\int_0^{+\infty} J_1(\lambda r)\sqrt{\lambda^2-k_2^2}\frac{e^{z\sqrt{\lambda^2-k_2^2}-h\sqrt{\lambda^2-k_0^2}}}{k_2^2\sqrt{\lambda^2-k_0^2}+k_0^2\sqrt{\lambda^2-k_2^2}}\lambda^2 d\lambda$$

$$E_z^2 = -\frac{j\omega\mu_0 I_0 l}{2\pi}\int_0^{+\infty} J_0(\lambda r)\frac{e^{z\sqrt{\lambda^2-k_2^2}-h\sqrt{\lambda^2-k_0^2}}}{k_2^2\sqrt{\lambda^2-k_0^2}+k_0^2\sqrt{\lambda^2-k_2^2}}\lambda^3 d\lambda$$

In medium 1, decomposition leads to three other equations in (6) which can be physically interpreted.

(6)

$$H_\phi^1 = \frac{I_0 l}{4\pi}\left[\frac{e^{-jk_0R}}{R}\left(jk_0\frac{r}{R}+\frac{r}{R^2}\right) - \frac{e^{-jk_0R'}}{R'}\left(jk_0\frac{r}{R'}+\frac{r}{R'^2}\right) + \int_0^{+\infty} J_1(\lambda r)e^{-(z+h)\sqrt{\lambda^2-k_0^2}}\frac{2k_2^2}{k_2^2\sqrt{\lambda^2-k_0^2}+k_0^2\sqrt{\lambda^2-k_2^2}}\lambda^2 d\lambda\right]$$

$$E_\rho^1 = \frac{j\omega\mu_0 I_0 l}{4\pi k_0^2}\left[\frac{e^{-jk_0R}}{R}\frac{r(z-h)}{R^2}\left(k_0^2-3j\frac{k_0}{R}-\frac{3}{R^2}\right) - \frac{e^{-jk_0R'}}{R'}\frac{r(z+h)}{R'^2}\left(k_0^2-3j\frac{k_0}{R'}-\frac{3}{R'^2}\right) - \int_0^{+\infty} J_1(\lambda r)e^{-(z+h)\sqrt{\lambda^2-k_0^2}}\frac{2k_2^2\sqrt{\lambda^2-k_0^2}}{k_2^2\sqrt{\lambda^2-k_0^2}+k_0^2\sqrt{\lambda^2-k_2^2}}\lambda^2 d\lambda\right]$$

$$E_z^1 = -\frac{j\omega\mu_0 I_0 l}{4\pi k_0^2}\left\{\frac{e^{-jk_0R}}{R}\left[k_0^2-\frac{jk_0}{R}-\frac{1+k_0^2(z-h)^2}{R^2}+\frac{3jk_0(z-h)^2}{R^3}+\frac{3(z-h)^2}{R^4}\right] - \frac{e^{-jk_0R'}}{R'}\left[k_0^2-\frac{jk_0}{R'}-\frac{1+k_0^2(z+h)^2}{R'^2}+\frac{3jk_0(z+h)^2}{R'^3}+\frac{3(z+h)^2}{R'^4}\right] + \int_0^{+\infty} J_0(\lambda r)e^{-(z+h)\sqrt{\lambda^2-k_0^2}}\frac{2k_2^2}{k_2^2\sqrt{\lambda^2-k_0^2}+k_0^2\sqrt{\lambda^2-k_2^2}}\lambda^3 d\lambda\right\}$$

Here, $R' = (r^2+(z+h)^2)^{1/2}$ is the distance between the image element at distance h below the plane and the observation point on Fig. 5.

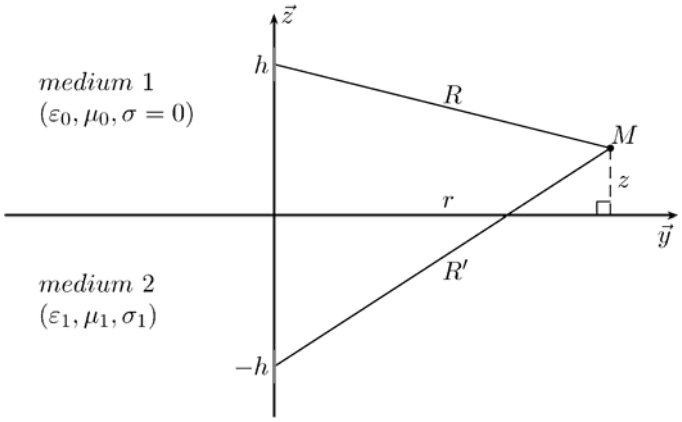

Fig. 5. Vertical z-directed current element source at height h and image at height $-h$ above perfectly conducting plane.

In (6), the components are expressed as the sum of three terms. The first represents a wave travelling directly from the current element I_0dl, the second is from a negative image - I_0dl and the third is called a surface wave term.

B. Numerical integration

The integrands in all components in both media are made up of three parts. The first element is the quotient whose denominator is $(k_0^2(\lambda^2-k_2^2)^{1/2}+k_2^2(\lambda^2-k_0^2)^{1/2})$. An oscillating term is created by spherical Bessel functions J_0 and J_1 and finally there is an exponential attenuation factor depending on the height of the dipole and the observation point.

Here, integral from z-directed electric field in (7) is studied but the same approach is correct for the other components of the electromagnetic field.

$$\int_0^{+\infty} J_0(\lambda r) e^{-(z+h)\sqrt{\lambda^2-k_0^2}} \frac{2k_2^2}{k_2^2\sqrt{\lambda^2-k_0^2}+k_0^2\sqrt{\lambda^2-k_2^2}} \lambda^3 d\lambda \qquad (7)$$

The denominator does not have special values because integration path of λ is the real axis. When the real and imaginary part of the integrand is plot for a distance *r*, one can observe four principle parts. The first one has low oscillations, the second is the most important because it has the most data. In fact, it is where the real part of $(k_0^2(\lambda^2-k_2^2)^{1/2}+k_2^2(\lambda^2-k_0^2)^{1/2}$ appears ($\lambda \approx k_0$). The third part is the effect of the Bessel Function because both real and imaginary values of integrand are oscillating. The last part is where the exponential is most important and it is negligible despite the oscillating behavior.

This analyze shows that different integration methods can be used for each part of the integrand. Third degree Newton-Cotes method is chosen for part one and three integrations and Gauss-Legendre quadrature with more than ten points is chosen for the integration of part two.

An adaptative integration algorithm was realized and tested for vertical component $\mathbf{E_z}$ over a medium wet soil, along the direction of propagation. Fig. 6. shows the comparison between three different methods, the numerical integration, the FDTD and integral equations computed with an industrial software FEKO. In the following, the integration algorithm will be named NISP which stand for Numerical Integration of Sommerfeld's Problem.

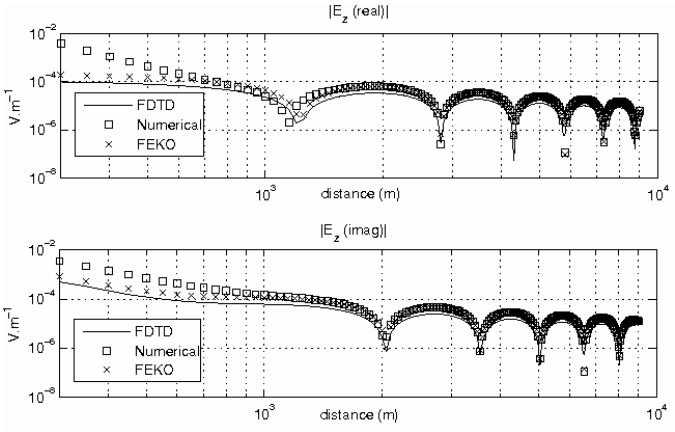

Fig. 6. Solution comparison of vertical electric component in Sommerfeld's problem.

C. NISP - 3D FDTD hybridisation

The main of this part is to compute the effect of a discontinuity in/on the soil with NISP – 3D FDTD hybridization. An object is placed in the far field of an infinitesimal vertical electric dipole. Incident electric $\mathbf{E_{inc}}$ and incident magnetic $\mathbf{H_{inc}}$ fields are computed around a cube with numerical integration algorithm and added as an incident wave source in the 3D FDTD. The situation with a homogeneous flat ground is shown on Fig 7.

First the Total Field / Scattered-Field technique is used with an object in the air to observe the scattering and validate the method and then a homogenous flat ground will be introduced. This part will be detailed in the presentation.

IV. CONCLUSIONS

The effects of natural environments in the near field and in the far field of antennas have been studied. First, FDTD is used to find a configuration where the system is more efficient and hybridization is realized with numerical integration in order to obtain the scattering of objects far from the source. The common use of these techniques will be helpful to better design LF antennas on irregular ground with emphasis on ground wave.

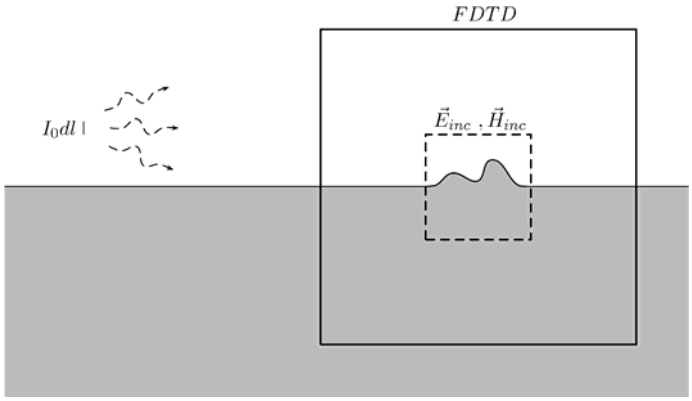

Fig. 7. NISP – 3D FDTD Hybridation. An infinitesimal vertical electric dipole creates electric and magnetic fields ($\mathbf{E_{inc}}$, $\mathbf{H_{inc}}$).

REFERENCES

[1] Taflove, A. and Hagness, S. C., "The Finite-Difference Time Domain Method," 3rd edition, Artech House, 2005.

[2] Zhou, L., Xi, X., Liu, J. and Yu, N. "LF Ground-Wave Propagation Over Irregular Terrain," Antennas and Propagation, IEEE Transactions on, Vol. 59, No. 4, 1254–1260, April 2011.

[3] Holland, R. and Simpson, L., "Finite-Difference Analysis of EMP Coupling to Thin Struts and Wires," Electromagnetic Compatibility, IEEE Transactions on , Vol. EMC-23, No. 2, 88–97, May 1981.

[4] Gedney, S. D., "An Anisotropic Perfectly Matched Layer Absorbing Medium for the Truncation of FDTD Lattices," Antennas and Propagation, IEEE Transactions on , Vol. 44, No. 12, 1630–1639, December 1996.

[5] Tewari, R. K., Swarup, S. and Roy, M. N., "Evaluation of Relative Permittivity and Conductivity of Forest Slab from Experimental Measured Data on Lateral Wave Attenuation Constant," International Journal of Electronics , Vol. 61, 597–605, November 1996.

[6] Sommerfeld, A., "Propagation of Waves in Wireless Telegraphy," Annalen der Physik , Vol. 28, 665–736, March 1909.

[7] Wu, Z. and MacLean, T., "Radiowave Propagation Over Ground," London U.K. : Chapman and Hall, 1993